



Full Text View

[Volume 30, Issue 1 \(January 2000\)](#)

Journal of Physical Oceanography

Article: pp. 40–50 | [Abstract](#) | [PDF \(2.70M\)](#)

The Atmospheric Boundary Layer above the Agulhas Current during Alongcurrent Winds

M. Rouault, A. M. Lee-Thorp, and J. R. E. Lutjeharms

Department of Oceanography, University of Cape Town, Rondebosch, South Africa

(Manuscript received July 22, 1998, in final form February 8, 1999)

DOI: 10.1175/1520-0485(2000)030<0040:TABLAT>2.0.CO;2

ABSTRACT

The response of the marine atmospheric boundary layer to the strong sea surface temperature (SST) gradient across the warm Agulhas Current was studied in the Agulhas Current Air–Sea Exchange Experiment, south of Port Alfred, South Africa. Shipboard meteorological and oceanographic measurements and radiosonde ascents are used to describe this response for wind regimes that are approximately parallel to the current. Surface heat fluxes increased by over 200 W m^{-2} from the shelf to the current while the sensible heat flux reversed sign. A characteristically stable boundary layer over the cool shelf waters was replaced by an unstable convective boundary layer over the current. The mean specific humidity and potential temperature of the boundary layer increased significantly over the current by 25% and 10% with a concomitant boundary layer deepening of $40 \text{ m } (^{\circ}\text{C})^{-1}$ SST. In the presence of alongcurrent winds an atmospheric moisture and thermal front developed over the inshore SST front. This is attributed to the horizontal gradient in the surface heat fluxes. The strong SST front owes its presence here to the juxtaposition of the warm current and an inshore kinematically driven subsurface upwelling cell whose surface expression is modulated by the wind stress.

1. Introduction

The Agulhas Current is considered to be the major western boundary current in the Southern Hemisphere ([Gordon 1986](#)). It forms the western limb of an anticyclonic subtropical gyre in the south Indian Ocean. The current is between 1000 and 1500 m deep, between 90 and 100 km wide, and may exhibit speeds even in excess of 2.5 m s^{-1} . With few exceptions, the current closely follows the continental shelf until the

Table of Contents:

- [Introduction](#)
- [The experiment](#)
- [Measurements and methods](#)
- [Background and meteorological](#)
- [Results](#)
- [Discussion](#)
- [Conclusions](#)
- [REFERENCES](#)
- [TABLES](#)
- [FIGURES](#)

Options:

- [Create Reference](#)
- [Email this Article](#)
- [Add to MyArchive](#)
- [Search AMS Glossary](#)

Search CrossRef for:

- [Articles Citing This Article](#)

Search Google Scholar for:

- [M. Rouault](#)
- [A. M. Lee-Thorp](#)
- [J. R. E. Lutjeharms](#)

latitude of Port Elizabeth. Near Port Elizabeth, the continental shelf widens to form the Agulhas Bank resulting in the formation of shear edge features such as eddies, plumes, and filaments on the inshore edge of the current ([Lutjeharms 1981](#)). In this region, cool waters are found over the continental shelf lying inshore of the 200-m isobath where intermittent upwelling gives rise to substantial temperature differences between the coastal waters and the Agulhas Current. It is in this context that one can expect to find variations in the marine atmospheric boundary layer (MABL) similar to variations observed in other areas with strong horizontal gradients in sea surface temperature such as the Gulf Stream or the Kuroshio Current.

[Sweet et al. \(1981\)](#) found variations in sea state, atmospheric lapse rate, and wind speeds across the north wall of the Gulf Stream. The atmospheric mixed layer increased by 300 to 400 m on the warm side. When the wind blew from the cold side to the warm side, the wind speed increased over the warm water. Similar results have been obtained in the Greenland Sea ([Vihma et al. 1991](#)), the Korean Strait ([Hsu 1984](#)), and the Agulhas Retroflexion area ([Mey et al. 1990](#)). [Hsu \(1988\)](#) has observed the development of an internal boundary layer when the wind blew from the cold to warm side and the generation of a sea-breeze-like circulation when the geostrophic wind was $\leq 5 \text{ m s}^{-1}$.


In the Joint Air–Sea Interaction (JASIN) Experiment [Guymer et al. \(1983\)](#) observed that fluxes are modulated by mesoscale patterns in SST. In winter 1986, the Genesis of Atlantic Lows Experiment (GALE) utilized aircraft, ship, and satellite observations to study the interaction between atmosphere and ocean, at all scales, off North Carolina ([Bane and Osgood 1989](#)). Extreme values of the latent and sensible heat flux (1000 W m^{-2}) were observed above the Gulf Stream. The high quality GALE dataset led to numerous modeling and case studies with an emphasis on mesoscale meteorology and extratropical winter cyclones ([Warner et al. 1990](#); [Holt and Raman 1992](#); [Doyle and Warner 1993](#); [Xie et al. 1996](#); [Reddy and Raman 1994](#)). The Frontal Air–Sea Interaction Experiment (FASINEX) was designed to study the ocean–atmosphere interaction across a sharp SST front. [Friehe et al. \(1991\)](#) studied the modification of the MABL when the wind was perpendicular to the sea surface temperature front. When the wind blew from the cold to the warm side, surface stability changed to unstable and the boundary layer became convective and more humid. When the wind blew from the warm to the cold side surface stability became stable or near-neutral with a decrease in wind speed. [Khalsa and Greenhut \(1989\)](#) presented evidence of secondary circulations, variations in the rates of entrainment and overturning at the top of the boundary layer.

The MABL is of substantial interest in the South African context since a better understanding of this layer is needed to comprehend how ocean–atmosphere interactions in the Agulhas Current system modulate South African weather and climate variability ([Rouault and Lutjeharms 1994](#)). Links between the warm waters of the Agulhas Current system and the summer climate of the subcontinent have been established ([Walker 1990](#); [Mason 1995](#)). Summer rainfall on the southeast coast of southern Africa has been shown to be significantly influenced by the proximity and temperature of the adjacent Agulhas Current ([Jury et al. 1993](#)). In summer, above normal rainfall was linked to an anomalously warm Agulhas Current. Latent heat fluxes and moisture convergence over the interior increase significantly when SSTs are 1°C above normal ([Walker 1990](#)). The first observations made from aircraft within this region ([Jury and Courtney 1991](#)) have revealed a spatially organized thermodynamic and kinematic atmospheric structure during uniform, light, westerly flow (approximately parallel to the current) ([Jury 1994](#)). It has been shown that this may even lead to substantial cumulus cloud, development over stretches of hundreds of kilometers along the current ([Lutjeharms et al. 1986](#); [Lee-Thorp et al. 1998](#)).

[Jury \(1995\)](#) has proposed that the preconditioning of the marine environment by SST plays a key role in the convective potential of transient weather systems. This may be important since the major-axis wind component for the region of the southeast coast is parallel to the coast (and consequently parallel to the Agulhas Current) ([Schumann 1989](#)). An adequate description of the structure and quantification of moisture in the boundary layer above the Agulhas Current during these conditions is clearly called for.

In this paper we set out to characterize and quantify the principal spatial characteristics of the MABL above the Agulhas Current during such alongcurrent winds. Shipboard meteorological and oceanographic measurements and radiosonde ascents were made during the Agulhas Current Air–Sea Exchange Experiment, the first experiment of its kind in these waters. The experimental design ([section 2](#)), data sampling and analysis ([section 3](#)), and background ([section 4](#)) are briefly described. In [section 5](#) we present the surface turbulent fluxes and atmospheric profiles that illustrate the response of the MABL to the strong SST front.

2. The experiment

The Agulhas Current Air–Sea Exchange Experiment (ACASEX) was designed to investigate atmospheric variations across the Agulhas Current and the potential influence of the atmosphere on the Agulhas Current and adjacent upwelling cell ([Rouault et al. 1995](#)). The region south of Port Alfred, an area sufficiently removed from the coast so as to avoid coastal influences, was chosen as the location for the experiment ([Fig. 1](#) ). This coastal region exhibits very intense, but localized, upwelling inshore of the Agulhas Current creating extreme horizontal SST gradients not found elsewhere. ACASEX consisted of a special research cruise aboard the R/V *Algoa* off Port Alfred and Port Elizabeth for the period 21

April to 3 May 1995. Twenty-four transects in the Agulhas Current were carried out in a mostly triangular cruise pattern. At least two transects were completed each day. Continuous surface meteorological measurements were undertaken in conjunction with radiosondes, which were launched approximately four times a day. These ascents were timed to coincide with periods when the vessel was over the shelf, SST front, current core, and seaward regions, where possible. Oceanographic measurements using expendable bathythermograph probes (XBTs) and an acoustic Doppler current profiler (ADCP) were carried out in support of this program. Standard, twice-daily radiosonde ascents made by the South African Weather Bureau at Port Elizabeth provided a land-based reference to assess the differences between the land and marine air masses.

3. Measurements and methods

a. Measurements

The wind speed and direction from a Furuno FW-200 aerovane-type anemometer, 22 m above the sea, were corrected for the ship's movement with a Global Positioning System (GPS). It compared favourably with the wind speed from a fast-response Gill sonic anemometer. Air temperature was measured at 16 m with an Aandera 3145 temperature sensor and SST was given by a SEACAT SBE 21 thermosalinograph at the ship's seawater intake at a depth of 2 m. Relative humidity was supplied by a Vaisala HMP35D, a slow response relative humidity (RH) sensor, and compared with the humidity from a fast-response Ophir infrared hygrometer, which also provided slow-response temperature measurements. These fast-response humidity measurements rapidly became unreliable due to sea-salt degradation of this device. A data acquisition system sampled these devices at 10-s intervals. The values obtained were averaged in 10-min bins and stored with relevant information such as time, latitude, longitude, ship speed, heading from a GPS, and sea level pressure.

The current velocity was measured with an RD ADCP. Data was recorded in a series of 8-m depth bins down the water column. The current velocity values used in this study are 20-min means of data obtained at a 16-m depth. Over depths greater than 1500 m the ADCP received bad data. This means that we have current speed data only from the shelf to the inner side of the Agulhas Current core. Therefore we assume (after [Pearce 1977](#)) that the current velocity in the core of the Agulhas Current is constant and then decreases linearly offshore.

The Vaisala RS80 Omega Sounding System provided vertical profiles of temperature and relative humidity at a resolution of 4 mb (roughly 50 m). Rawinsonde wind were not available. At the beginning of the experiment water entered the housing enclosing the tracking antenna preamplifier with the result that the tracking signal could not be received.

b. Methods

The turbulent fluxes of momentum and sensible and latent heat have been calculated using the bulk method algorithm developed by [Fairall et al. \(1996\)](#) for TOGA COARE. The bulk formulas for wind stress, sensible heat, and water vapor fluxes are

$$\begin{aligned}\tau &= \rho_a C_D (U - U_s)^2 \\ Q_H &= \rho_a c_p C_H (U - U_s) (T_s - \Theta) \\ Q_E &= \rho_a C_E (U - U_s) (q_s - q),\end{aligned}$$

where U and q are mean wind speed and specific humidity measured at 22 and 17 m. Near the surface,

$$\Theta = T_a + 0.0098z_r,$$

where T_a is the air temperature measured at $z_r = 16$ m; U_s is the sea surface current speed and cannot be neglected.

Current speeds of up to 2 m s^{-1} were measured during ACASEX ([Rouault et al. 1995](#)). For example, neglecting the current speed at a wind speed of 4 m s^{-1} will lead to a 50% error in the latent heat flux. Here ρ_a is the air density, and T_s and q_s are the mean sea surface temperature and specific humidity at the surface; q_s is calculated from q_{sat} the saturation specific humidity at the sea surface temperature

$$q_s = 0.98q_{\text{sat}}(T_s).$$

The factor 0.98 is introduced to account for the reduction in vapor pressure due to salinity ([Fairall et al. 1996](#)). C_d is the

drag coefficient, and C_H and C_E are the dimensionless Stanton and Dalton numbers, also called transfer coefficients for heat and water vapor. The algorithm iterates on the Monin–Obukhov length, L . This is the ratio of the work done by or against the buoyant turbulent forces to the rate of shear production of turbulent energy. Then

$$\zeta_{10} = 10/L$$

is the atmospheric stability parameter at 10 m, positive for stable conditions and negative for unstable conditions.

The model of [Fairall et al. \(1996\)](#) is based on that of [Liu et al. \(1979\)](#). It includes a separate module to calculate the actual sea surface temperature (skin temperature) from the measured sea surface temperature, which is usually made at the ship intake a few meters below the surface, the contribution of the sensible heat due to rainfall, a new relation for the roughness length, and a new parameterization for light wind and convective regimes.

Although our fast-response measurements make it possible to derive inertial dissipation estimates of the surface turbulent fluxes, we prefer to use the bulk method in order to produce a continuous turbulent flux time series. Recent studies using the inertial dissipation method discard results when the ship maneuvers, is not underway at full speed, or when the relative wind speed is not blowing within 30° of the bow (e.g., [Yelland and Taylor 1996](#)). This occurred frequently (e.g., every time a radiosonde was launched). Furthermore, the requirements of stationarity and horizontal homogeneity are violated above the SST front.

The virtual potential temperature is not just an attractive but necessary means of describing the structure of the boundary layer ([Stull 1988](#)). This is (in kelvin) for unsaturated air

$$\theta_v = \theta(1 + 0.61r),$$



where r is the mixing ratio. The atmospheric mixed layer (with top z_i) may then be defined as the layer above the surface where the virtual potential temperature profile is approximately adiabatic. In order to describe the mean scalar quantities of the boundary layer the following properties are defined (after [Katsaros et al. 1994](#)):

$$\begin{aligned}\bar{\theta}_e &= \frac{1}{z_i} \int_0^{z_i} \theta_e(z) dz \\ \bar{\theta} &= \frac{1}{z_i} \int_0^{z_i} \theta(z) dz \\ \bar{q} &= \frac{1}{z_i} \int_0^{z_i} q(z) dz,\end{aligned}$$

where z_i is the atmospheric mixed layer height and θ_e is the equivalent potential temperature ([Bolton 1980](#)).

The convective boundary layer may be defined as the layer above the surface that is convectively coupled to the surface. Over the ocean, the convective boundary layer plays an important role in regulating the upward transfer of heat and moisture ([Betts and Albrecht 1987](#)). This may be investigated using a conserved variable diagram (plot of one conserved variable against another), which distinguishes between mixing, radiative, and precipitation processes. Atmospheric profiles were composited for better statistical relevance.

4. Background and meteorological setting

We present results for two contrasting wind regimes (westerly and easterly) where the wind is parallel to the current. The spatial patterns described by these two case studies were reproduced during other transects when the wind was parallel to the current. For the “westerly” wind case on 24 April maritime weather conditions were influenced by a weak low pressure passing east of the subcontinent ([Fig. 2a](#) ). Light, westerly geostrophic winds were indicated. Observed west-southwesterly winds at the surface of $5\text{--}10\text{ m s}^{-1}$ were approximately parallel to the SST front. The easterly winds of the previous two days had exposed upwelling in the study region. At the SST front a gradient of $3^\circ\text{C}/10\text{ km}$ was observed. Shelf SSTs of 15°C compared with values found for the core of the current of $\leq 25^\circ\text{C}$. On 29 April, the “easterly” case, a ridging anticyclone ([Fig. 2b](#) ) brought easterly air flow (approximately parallel to the SST front).

5. Results

a. Oceanography

Satellite imagery was used to identify the location of the Agulhas Current and to show the position and intensity of the adjacent upwelling cell. The intermittent inshore intrusion of cold water above the continental shelf is due to local upwelling of water from a depth of between 200 to 600 m. The exact nature of this particular upwelling process is not well understood. Two candidate processes exist. Ekman transport in the bottom boundary layer of the Agulhas Current would in theory force water upward next to the continental slope as the swift current moves along the edge of the continental shelf. This has been observed (Schumann 1986). Furthermore, where the current trajectory passes from a narrow to a wide shelf, such as off Port Alfred, a distinct cell of topographically induced upwelling could be expected (Gill and Schumann 1979). Such upwelling has also been observed in this region. Since the resultant upwelling is thought to be driven by these two relatively invariant processes, the high degree of temperature variability at the sea surface on short timescales is unexpected.

The closely spaced temperature measurements taken during this cruise, repeated at intervals of only 5 days, present evidence for the most likely processes involved in this irregularity (Fig. 3). On 24 April the demarcation of isotherms clearly shows the movement of cold water upward along the shelf slope. Five days later this is even more evident with water colder than 12°C covering the ocean floor of the Agulhas Bank. This water is normally found at depths greater than 600 m at a distance of 60 km offshore. This kinematically driven upwelling was therefore observed on both days, but not so its surface expression. Prior to 24 April, strong, easterly winds predominated. On 24 April, a strong horizontal temperature gradient from 14° to 21°C was observed between the coast and the shelf edge. Five days later this had been replaced at the sea surface by a warm layer of uniform temperature between 20° and 21°C, about 15 m thick. Winds measured at sea during the cruise were predominantly from the southwest. Such winds would have caused an Ekman drift in the surface layers carrying surface water of the Agulhas Current toward the coast, thus covering the cold upwelled water with a thin layer of warmer water. In the process a strong thermocline was created. This expected Ekman drift was, in fact, observed and measured during the cruise with the ADCP (Rouault et al. 1995). These measurements show that although the deep, kinematic upwelling in the eastern Agulhas Bank upwelling cell may be persistent, continuously bringing nutrient-rich water onto the shelf, the surface expression of this process will only be evident intermittently due to local wind action.

b. Spatial variation of the surface fluxes

Results from a single transect on 29 April show that air–sea exchanges are closely correlated with SST (Fig. 4). The left portion of the plot corresponds to the shelf, center to the current and right to the seaward region. Highest fluxes correspond to the current, lowest to the inshore region. Over the cool shelf the air temperature is greater than the SST and ζ_{10} is positive (stable). This corresponds to downward sensible and lower latent heat fluxes (Table 1). A value for the latent heat flux of 78 W m⁻² coincides with the intrusion of warm Agulhas Current waters onto the shelf. We estimate an average latent heat flux for the shelf of 50 and 270 W m⁻² for the current, that is, a fivefold increase. This is for alongcurrent winds over the range of meteorological conditions (including a storm event) encountered. The surface stability changes sign at the inshore SST front as the SST exceeds the air temperature by 3°C, indicative of convective conditions. A dramatic increase in the latent heat flux occurs. A maximum turbulent heat flux of 347 W m⁻² above the current core is related to the wind speed increase. Immediately seaward of the current, the air–sea temperature difference decreases. Surface stability suppresses convection leading to negligible sensible heat and small latent heat fluxes. In general, this spatial pattern was reproduced during all transects. The latent heat flux constituted the main component (80%–90%) of the surface turbulent heat exchange over the current. Surface destabilization occurred across the inshore SST front, characterized by a large horizontal latent heat flux gradient.

c. Mean thermodynamic structure

The mean thermodynamic structure is a function of the surface turbulent fluxes and synoptic conditions. Composite plots of the atmosphere above the current for 24 April and 29 April in Fig. 5 reveal the mean structure of the convective boundary layer and free atmosphere. The conserved variable structure of the boundary layer is characterized by a straight line (mixing line) (Betts and Albrecht 1987) from the surface to the inversion where a θ_e – r kink is found. The boundary layer height (marked z_b) was independently determined from the θ_v profile (top panel) and therefore gives an unambiguous interpretation of this kink. Air below the subsidence inversion (SI) and above the boundary layer (z_b) appears to define a separate “mixing” line. Its semipermanence (we observed a variation to this structure only during a storm event) suggests that this is not a remnant of an earlier surface-based boundary layer. The θ profile of this layer approximately follows that of an air parcel originating from the base of the atmospheric mixed layer. We suggest that this second mixing line is associated with cloud-scale mixing (Lee-Thorp et al. 1998) and synoptic-scale subsidence. The subsidence inversion marks a θ_e reversal along which radiative cooling has occurred (Betts and Albrecht 1987) (i.e., subsiding air cools radiatively while its

mixing ratio, r , remains unchanged). This inversion has previously been erroneously identified as the boundary layer height (Mey et al. 1990, Fig. 6). A double-inversion structure is therefore apparent. A characteristic mixing line is found below a θ_e - r kink at the limit of dry adiabatic convection, z_p .

d. Spatial variation of the marine atmospheric boundary layer

If the predominant wind axis is parallel to the current with little cross-frontal advection, then it is reasonable to assume that the boundary layer above the shelf, current, and seaward region retain separate characteristics that are determined by the exchanges at the air-sea interface. This hypothesis can easily be tested using the data from the radiosonde ascents conducted during ACASEX. A pattern of transition from a convective boundary layer to a stable (or relatively more stable) one will be shown to be a central theme in all cases and is in close agreement with the increase in surface fluxes.

Figure 6 shows boundary layer differences between Port Elizabeth (PE) and seaward of the current for the third transect on 24 April during west-southwesterly winds. We have used nighttime data at PE to construct this cross section. The moisture profile at PE, however, was conserved and there is little difference between the daytime and nighttime humidity cross sections (upper panel). A dome of warm, moist air above the current extends to the height of the MABL top with dry air residing above the shelf and seaward of the current. (Recall that the current extends from 130 to 220 km offshore of PE.) In the vicinity of the shelf, the surface sensible heat flux is downward. A shallow (200 m), stable layer is capped by a strong inversion where the virtual potential temperature θ_v increases by 2°C over 200 m (Fig. 7). Above the current core, a well-mixed/neutral profile is attained. In this case, the profile is not as convective as might be expected due to small surface heat fluxes above the current associated with decreasing wind speeds. Beyond the current, on the seaward border, surface heat and momentum fluxes are negligible and a stable profile is attained. The spatial variation of \bar{q} , $\bar{\theta}$ and $\bar{\theta}_e$ is unambiguous (Table 2) with differences of 1.7 g kg⁻¹, 3°, and 6.5°C apparent between the shelf and current.

On 29 April, air-sea exchanges of heat and moisture were much larger, leading to a deeper MABL. Figure 8 follows the lower atmosphere during easterly winds (approximately parallel) to the SST front. Daytime data at Port Elizabeth has been used here. Differences in \bar{q} , $\bar{\theta}$, and $\bar{\theta}_e$ (Table 2) are somewhat deaccentuated due to the small cross-frontal wind component. Nevertheless a deep, moist, warm boundary layer over the current gives way to strong moisture contrasts on the inshore and offshore edges. An initially stable boundary layer (seaward front) is replaced by a convective boundary layer (current) and shallow convective boundary layer (shelf) with a concomitant deepening of 300 m over the current (Fig. 9). The convective nature of the boundary layer above the shelf is due to the small (but not insignificant) oceanic heat loss in this region.

e. Internal boundary layer

The varying synoptic conditions during ACASEX allowed an investigation of internal boundary layer (IBL) development when the wind blew from cold to warm (shelf to current) and from warm to cold (current to shelf or seaward of the current). Figure 10 traces this process. Airflow during the first transect on 24 April was westerly (approximately parallel to the isotherms but with a small cross-frontal component). At the inshore (offshore) SST front this component is from cold to warm (warm to cold). The stable shelf profile is “capped” by an inversion. Destabilization of the surface layer then occurs at the SST front as the first surface thermals mix vertically and a convective thermal internal boundary layer (TIBL) structure is formed. The TIBL top is sharp. Downwind (over the Agulhas Current core) the TIBL is less distinguishable. In this case the TIBL does not grow with fetch downstream due to diminishing surface heat fluxes and a decrease in the wind speed. Beyond the current, on the seaward border, surface heat and momentum fluxes were low and a stable internal boundary layer (SIBL) is formed.

6. Discussion

The analysis presented here has focused on quantification of the principal spatial structures with an emphasis on moisture uptake. With the exception of the composite analysis presented by Jury (1994) of aircraft cross sections during westerly, alongcurrent winds (Jury and Courtney 1991), scant attention has to date been paid to the structure of the boundary layer above the Agulhas Current. It was noted that maximum wind speed and atmospheric turbulence corresponded to the core of the current.

While Jury (1994) found that the MABL top on the cold side is approximately 600 m, 1000 m above the current, this description may be simplistic. The spatial heat flux gradient across the current sets up a transition in stability of the boundary layer. The variation of mixed layer height (growth ratio), z_p , is complicated by the difficulty in defining a mixed layer top for a stable boundary layer (Stull 1988, pp. 504–506) and the magnitude of the surface heat fluxes. Despite a strong SST gradient of 3°C/10 km, a shallow mixed layer was observed above the current on 24 April due to low heat fluxes. During alongcurrent winds it is apparent that the boundary layer structure becomes spatially organized in agreement with Jury

(1994). A dome of moist air above the current was replaced by dry air seaward and inshore of the current. Over the inshore SST front this transition defines an atmospheric moisture front whose depth is equal to the MABL height. Such coastal fronts have been observed elsewhere where the wind is sufficiently parallel to the coastline. Under such conditions latent heat release is localized and preconditioning of the marine environment occurs. The orientation of the wind is important. Thermodynamic differences were emphasized when the component of airflow across the SST front was minimized. For example, on an occasion of east-northeasterly winds (parallel to the inshore SST front) on 30 April a mean humidity difference of over 3 g kg^{-1} was observed in the presence of an even stronger moisture front. This is in direct contrast to the case where the wind blows onshore, perpendicular to the current (Lee-Thorp et al. 1999). A progressive accumulation of MABL moisture was accompanied by a consistent deepening of the humidity mixed layer. The MABL deepened rapidly as air moved from the seaward region over the current, becoming shallow and stable over the shelf where a deep residual moisture layer acted as a tracer of the former vertical extent of convective eddies.

Alternating westerly and easterly wind stress facilitates onshore and offshore Ekman transport in the oceanic surface layer. This may control the variability in strength and position of the inshore SST front, which in turn has implications for surface exchanges across the inshore SST front. XBT results have shown that kinematically driven upwelling by the Agulhas Current may prime the system. Lower SSTs over the shelf region on 24 April were related to the easterly wind stress of the previous two days. Westerly wind stress and onshore Ekman transport brought a subsequent reduction in intensity of the SST front ($2^\circ\text{C}/10 \text{ km}$) by 29 April. A progressive intensification of the SST gradient then occurred during easterly wind stress such that a gradient in SST of $3.5^\circ\text{C}/10 \text{ km}$ was observed by 30 April. An unambiguous wind speed increase over the current and decrease over the shelf and seaward region was observed to occur only on 30 April during winds parallel to the axis of the SST front and an intense SST front. Possible mechanisms are to be found in mesoscale circulations and/or differential turbulent mixing of high-momentum upper air. It is not possible to address this question with the available dataset.

7. Conclusions

The response of the MABL to the sharp SST contrast on the inshore edge of the warm Agulhas Current was investigated in the Agulhas Current Air–Sea Exchange Experiment. The background weather for our investigation was characterized by alongcurrent flow, either as cool westerly winds or as warm easterly winds typical of winter cyclonic and summer anticyclonic conditions respectively.

The results may be summarized as follows:

1. While kinematic upwelling due to the Agulhas Current may prime the eastern Agulhas Bank upwelling cell, its surface manifestation is controlled by alternating wind stress and resultant Ekman transport of the surface waters. Upwelling-favorable winds are from the east.
2. Large horizontal gradients of the surface heat fluxes, especially the latent heat flux occur. The surface latent heat flux increased on average by a factor of 5 over the current while the sensible heat flux reversed sign. Surface stability changed sign at the inshore SST front.
3. This large horizontal gradient in the surface heat fluxes sets up a transition in stability of the boundary layer. Owing to the difficulty in defining a stable boundary layer top, the increase in MABL depth was sometimes ambiguous. We estimate a boundary layer depth to SST growth ratio of approximately $40 \text{ m } (^\circ\text{C})^{-1}$.
4. An atmospheric moisture front occurs in the boundary layer across the inshore sea surface temperature front during alongcurrent winds. A dome of moisture above the current indicated that latent heating was localized with little cross-frontal advection. The mean specific humidity of the MABL increased by approximately 25% [or $0.35 \text{ (g kg}^{-1}) (^\circ\text{C})^{-1}$] SST.
5. The atmosphere contained two inversions. The first inversion capped the boundary layer and limits dry adiabatic convection. The second, higher-level inversion was associated with synoptic-scale subsidence.
6. When the wind had a component across the sea surface temperature front, the development of an internal boundary layer was observed. The internal boundary layer was convective for air blowing from cold to warm and stable for air blowing from warm to cold.

The Agulhas Current has frequently been linked to South African climate. Thus an emphasis has been placed here on a useful quantification and characterization of the atmospheric boundary layer. These results support the hypothesis that substantial preconditioning of the marine atmospheric environment occurs in the vicinity of the Agulhas Current.

The authors wish to thank the South African Weather Bureau, especially Sidney Marais and Piet King, and the Sea Fisheries Research Institute for making shiptime and data available. The financial support of the Foundation for Research Development and the Water Research Commission is gratefully acknowledged. Special thanks to Chris Fairall, Jim Edson, and Ken Davidson for sharing their softwares. Isabel Ansorge and Mark Majodina are acknowledged.

REFERENCES

- Bane, J. M., Jr., and K. E. Osgood, 1989: Wintertime air–sea interaction process across the Gulf Stream. *J. Geophys. Res.*, **94**, 10 755–10 772..
- Betts, A. K., and B. A. Albrecht, 1987: Conserved variable analysis of the convective boundary layer thermodynamic structure over the tropical oceans. *J. Atmos. Sci.*, **44**, 83–99.. [Find this article online](#)
- Bolton, D., 1980: The computation of equivalent potential temperature. *Mon. Wea. Rev.*, **108**, 1046–1053.. [Find this article online](#)
- Brown, R. A., and R. C. Foster, 1994: On PBL models for general circulation models. *J. Global Atmos.–Ocean Syst.*, **2**, 163–183..
- Doyle, J., and T. T. Warner, 1993: Nonhydrostatic simulations of coastal mesobeta-scale vortices and frontogenesis. *Mon. Wea. Rev.*, **121**, 3371–3392.. [Find this article online](#)
- Fairall, C. W., E. F. Bradley, D. P. Rogers, J. B. Edson, and G. S. Young, 1996: Bulk parametrization of air–sea fluxes for Tropical Ocean–Global Atmosphere Coupled–Ocean Atmosphere Response Experiment. *J. Geophys. Res.*, **101**, 3747–3764..
- Friehe, C. A., and Coauthors, 1991: Air–sea fluxes and surface layer turbulence around a sea surface temperature front. *J. Geophys. Res.*, **96**, 8593–8609..
- Gill, A. E., and E. H. Schumann, 1979: Topographically induced changes in the structure of an inertial coastal jet: Application to the Agulhas Current. *J. Phys. Oceanogr.*, **9**, 975–991.. [Find this article online](#)
- Gordon, A. L., 1986: Inter-ocean exchange of thermocline water. *J. Geophys. Res.*, **91**, 5037–5046..
- Guymer, T. H., J. A. Businger, K. B. Katsaros, W. J. Shaw, P. K. Taylor, W. G. Large, and R. E. Payne, 1983: Transfer processes at the air–sea interface. *Philos. Trans. Roy. Soc. London, Series A*, **308**, 253–273..
- Holt, T., and S. Raman, 1992: Three-dimensional mean and turbulence structure of a coastal front influenced by the Gulf Stream. *Mon. Wea. Rev.*, **120**, 17–39.. [Find this article online](#)
- Hsu, S. A., 1984: The effect of cold-air advection on internal boundary-layer development over warm oceanic currents. *Dyn. Atmos. Oceans.*, **8**, 307–319..
- , 1988: *Coastal Meteorology*. Academic Press, 260 pp..
- Jury, M. R., 1994: A thermal front within the atmospheric boundary layer over the Agulhas Current south of Africa: Composite aircraft observations. *J. Geophys. Res.*, **99**, 3297–3304..
- , 1995: A review of research on ocean–atmosphere interactions and South African climate variability. *S. Afr. J. Sci.*, **91**, 289–294..
- , and S. Courtney, 1991: A transition in weather over the Agulhas Current. *S. Afr. J. Mar. Sci.*, **10**, 159–171..
- , H. R. Valentine, and J. R. E. Lutjeharms, 1993: Influence of the Agulhas Current on summer rainfall along the southeast coast of South Africa. *J. Appl. Meteor.*, **32**, 1282–1287.. [Find this article online](#)
- Katsaros, K. B., M. A. Donelan, W. M. Drennan, and K. M. Howard, 1994: Surface fluxes and their relation to planetary boundary layer structure. *Proc. Air–Sea Interface Symp., Radio and Acoustic Sensing, Turbulence and Wave Dynamics*, Marseilles, France, CNRS, 124..
- Khalsa, S. J., and G. K. Greenhut, 1989: Atmospheric turbulence structure in the vicinity of an oceanic front. *J. Geophys. Res.*, **94**, 4913–4922..
- Lee-Thorp, A. M., M. Rouault, and J. R. E. Lutjeharms, 1998: Cumulus formation above the Agulhas Current: A case study. *S. Afr. J. Sci.*, **94**, 351–354..

- , —, and —, 1999: Moisture uptake above the Agulhas Current: A case study. *J. Geophys. Res.*, **104**, 1423–1430..
- Liu, W. T., K. B. Katsaros, and J. A. Businger, 1979: Bulk parametrization of air–sea exchanges of heat and water vapor including the molecular constraints at the interface. *J. Atmos. Sci.*, **36**, 1722–1734.. [Find this article online](#)
- Lutjeharms, J. R. E., 1981: Spatial scales and intensities of circulation in the ocean areas adjacent to South Africa. *Deep-Sea Res.*, **28**, 1289–1302..
- , R. D. Mey, and I. T. Hunter, 1986: Cloud lines over the Agulhas Current. *S. Afr. J. Sci.*, **82**, 635–640..
- Mason, S. J., 1995: Sea surface temperature—South African rainfall associations, 1910–1989. *Int. J. Climatol.*, **15**, 119–135..
- Mey, R. D., N. D. Walker, and M. R. Jury, 1990: Surface heat fluxes and marine boundary layer modification in the Agulhas Retroflexion Region. *J. Geophys. Res.*, **95**, 15 997–16 015..
- National Academy of Sciences, 1992: A review of the state of the science. *Coastal Meteorology*, National Academy Press, 26–27..
- Pearce, A. F., 1977: Some features of the upper 500 m of the Agulhas Current. *J. Mar. Res.*, **35**, 731–751..
- Reddy, N. C., and S. Raman, 1994: Observations of a mesoscale circulation over the Gulf Stream Region. *Global Atmos.–Oceans Syst.*, **2**, 21–40..
- Rouault, M., and J. R. E. Lutjeharms, 1994: Air–sea interaction in the marine atmospheric boundary layer: A new South African research venture. *S. Afr. J. Sci.*, **90**, 11–12..
- , A. M. Lee-Thorp, I. Ansorge, and J. R. E. Lutjeharms, 1995: The Agulhas Current Air–Sea Exchange Experiment. *S. Afr. J. Sci.*, **91**, 493–496..
- Schumann, E. H., 1986: The bottom boundary layer inshore of the Agulhas Current off Natal in August 1975. *S. Afr. J. Mar. Sci.*, **4**, 93–102..
- , 1989: The propagation of air pressure and wind systems along the South African coast. *S. Afr. J. Sci.*, **85**, 382–385..
- Stull, R. B., 1988: *An Introduction to Boundary Layer Meteorology*. Kluwer Academic, 666 pp..
- Sweet, W., R. Fett, J. Kerling, and P. LaViolette, 1981: Air–sea interaction effects in the lower troposphere across the north wall of the Gulf Stream. *Mon. Wea. Rev.*, **109**, 1042–1052.. [Find this article online](#)
- Vihma, T., J. Launiainen, and G. Krause, 1991: On the air–sea interaction in areas of thermal marine fronts in the Greenland Sea. *Atmos.–Oceans*, **29**, 596–610..
- Walker, N. D., 1990: Links between South African rainfall and temperature variability of the Agulhas and Benguela Current systems. *J. Geophys. Res.*, **95**, 3297–3319..
- Warner, T. T., M. N. Lakhtakia, J. Doyle, and A. Pearson, 1990: Marine atmospheric boundary layer circulation forced by Gulf Stream sea surface temperature gradients. *Mon. Wea. Rev.*, **118**, 309–323.. [Find this article online](#)
- Xie, L., L. J. Pietrafesa, and S. Raman, 1996: Mesoscale air–sea interaction over the continental shelf off the Carolina coast. *Global Atmos.–Oceans Syst.*, **4**, 65–88..
- Yelland, M., and P. K. Taylor, 1996: Wind stress measurement from the open ocean. *J. Phys. Oceanogr.*, **26**, 541–558.. [Find this article online](#)

Tables

Table 1. Turbulent air–sea exchanges on 29 Apr. Averages are given for the shelf and Agulhas Current. Q_T is the total turbulent heat flux ($Q_T = Q_H + Q_E$), Unit: W m^{-2} . The quantity $d\text{SST}/dy$ is the horizontal gradient of sea surface temperature ($^\circ\text{C}/\text{km}$) perpendicular to the inshore SST front (i.e., between the shelf and current). Unit for $(\tau)^{1/2}$ is N m^{-2} .

	$\bar{\tau}$	\bar{Q}_H	\bar{Q}_E	\bar{Q}_T	$\max(Q_T)$	$\bar{\zeta}_{10}$	$d\text{SST}/dy$
Shelf	0.14	-5	78	73	102	0	0.2
Agulhas Current	0.2	44	252	296	347	-0.2	

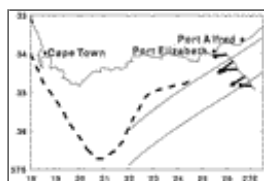
[Click on thumbnail for full-sized image.](#)

Table 2. Summary of mean boundary layer differences between the current core and the shelf for selected cases of alongcurrent winds and grouped according to degree of alongshore transport. Entries in bold are discussed in the text.

	ΔSST (°Ckm)	Δz (m)	$\Delta \rho$ (kg ⁻¹)	$\Delta \rho$ (°C)	$\Delta \rho$ (°C)	Comments
24 Apr, third transect	3.0	150	1.7	3.0	6.5	WSW winds, parallel
30 Apr	3.5	200	3.3	1.0	10.8	ENE winds, parallel
1 May	3.5	200 (ambiguous)	4.0	3.6	15.8	WSW winds, parallel
24 Apr, second transect	3.0	(ambiguous)	1.3	1.6	5.7	W winds, = parallel
29 Apr	2.0	300	1	1	4.0	E winds, = parallel

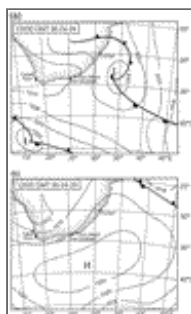
[Click on thumbnail for full-sized image.](#)

Figures



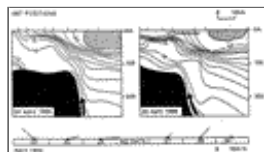
[Click on thumbnail for full-sized image.](#)

Fig. 1. Reference map showing an example transect (thin line) and winds (bold) on 29 Apr and the edges of the Agulhas Current (thin parallel lines). The inshore edge of the current follows the 200-m isobath (dashed).



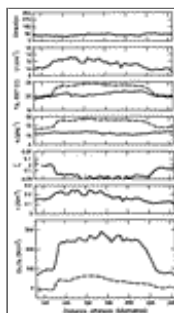
[Click on thumbnail for full-sized image.](#)

Fig. 2. Synoptic chart (a) at 1200 UTC 24 Apr 1995 (a) and (b) at 1200 UTC 29 Apr.



[Click on thumbnail for full-sized image.](#)

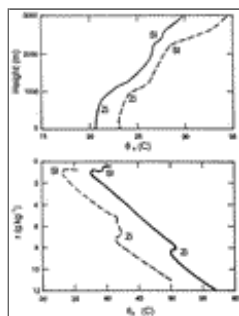
Fig. 3. Changes in the eastern Agulhas Bank upwelling cell as seen in temperature sections taken five days apart (after Rouault et al. 1995). Solid arrows indicate inferred bottom Ekman transport; an open arrow the surface Ekman flux due to the wind. The surface core of the Agulhas Current, consisting of water warmer than 24°C, is shaded. Winds observed on location are shown in the bottom panel. Lines denote the direction toward which the air moved.



[Click on thumbnail for full-sized image.](#)

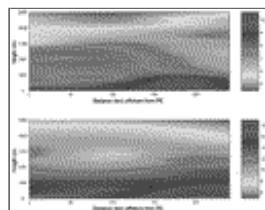
Fig. 4. Air-sea exchanges at the surface vs distance offshore on 29 Apr for the transect in Fig. 1. The parameters (from top to bottom) are: wind direction and wind speed at 10 m, air temperature at 10 m (solid), and sea surface skin temperature (dashed);

specific humidity at 10 m (solid) and saturation specific humidity at the sea surface (dashed); stability parameter, $\zeta_{10} = 10/L$ (solid); wind stress (solid); latent heat flux (solid) and sensible heat flux (dashed). Labels on the horizontal axis give the distance, in kilometers, from Port Elizabeth. The current extends from 130 to 220 km offshore.



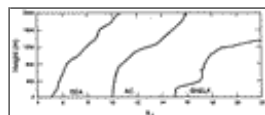
Click on thumbnail for full-sized image.

Fig. 5. Composite plots of the atmospheric structure on 24 Apr (solid) and 29 Apr (dashed). The upper panel shows the composite θ_v profiles; the lower panel the corresponding conserved variable diagram of the mixing ratio r and equivalent potential temperature θ_e . The r axis has been inverted so that the plot superficially represents a θ_e -height plot. The boundary layer top (z_b) and subsidence inversion (SI) are indicated.



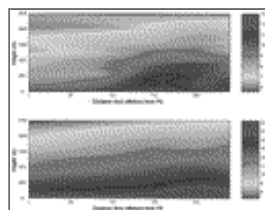
Click on thumbnail for full-sized image.

Fig. 6. Boundary layer modification on 24 Apr during west-southwesterly winds. The horizontal axes of the color contour plots of specific humidity (upper panel) and temperature (lower panel) show the distance from Port Elizabeth (PE) in kilometers. A nighttime radiosonde release has been used for this cross section. The wind can be visualized as blowing into the page. Values of specific humidity (g kg^{-1}) and air temperature ($^{\circ}\text{C}$) are given by each color bar.



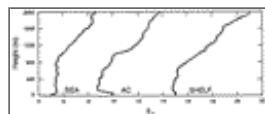
Click on thumbnail for full-sized image.

Fig. 7. Boundary layer structure on 24 Apr at the specified locations shown, namely, the shelf, current, and sea. The individual traces of θ_v are from the same transect as in [Fig. 6](#) and have been offset to aid visualization.



Click on thumbnail for full-sized image.

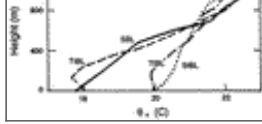
Fig. 8. Same as [Fig. 6](#) but for 29 Apr during easterly winds. The wind can be visualized as blowing out of the page.



Click on thumbnail for full-sized image.

Fig. 9. Same as [Fig. 7](#) but for 29 Apr.





[Click on thumbnail for full-sized image.](#)

Fig. 10. Internal boundary layer formation on 24 Apr. This transect was undertaken before that from [Fig. 6](#). The wind may be visualized as blowing from left to right. A stable boundary layer (SBL) over the shelf (____) is replaced by a convective thermal internal boundary layer (TIBL) (– – –), which decays downstream ([bu75]). Seaward of the current a stable internal boundary layer (SIBL) forms (·····).

Corresponding author address: Dr. Mathieu Rouault, Department of Oceanography, University of Cape Town, Rondebosch 7701, South Africa.

E-mail: rouault@physci.uct.ac.za

[top ▲](#)



© 2008 American Meteorological Society [Privacy Policy and Disclaimer](#)
Headquarters: 45 Beacon Street Boston, MA 02108-3693
DC Office: 1120 G Street, NW, Suite 800 Washington DC, 20005-3826
amsinfo@ametsoc.org Phone: 617-227-2425 Fax: 617-742-8718
[Allen Press, Inc.](#) assists in the online publication of *AMS* journals.